

Regulating the Product Distribution of CO Reduction by the Atomic-Level Structural Modification of the Cu Electrode Surface

Youn-Geun Kim¹ · Alnald Javier¹ · Jack H. Baricuatro¹ · Manuel P. Soriaga^{1,2}

Published online: 7 June 2016

© Springer Science+Business Media New York 2016

Abstract Cu catalyzes the electrochemical reduction of CO₂ or CO to an assortment of products, a behavior that is a detriment when only one reduced compound is desired. The present article provides an example in which, through the atomic-level control of the structure of the Cu electrode surface, the yield distribution is regulated to generate only one product. The reaction investigated was the preferential reduction of CO to C₂H₅OH on Cu at a low overpotential in alkaline solution. Experimental measurements combined electrochemical scanning tunneling microscopy (ECSTM) and differential electrochemical mass spectrometry (DEMS). An atomically ordered Cu(100) surface, prepared from either a single crystal or by Cu(pc)-to-Cu(100) reconstruction, did not produce ethanol. When the surfaces were subjected to monolayer-limited Cu↔Cu₂O cycles, only the reconstructed surface underwent an additional structural transformation that spawned the selective production of ethanol at a potential 645 mV *lower* than that which generates multiple products. *Quasi-operando* ECSTM indicated transformation to an ordered stepped surface, Cu(S)–[3(100)×(111)], or Cu(511). The non-selective, multiple-product Cu-catalyzed reduction of CO had thus been regulated to yield only one liquid fuel by an atomic-level structural modification of the electrode surface.

Keywords Selective reduction of CO to ethanol on Cu(511) in alkaline solution at low overpotential · *Operando* generation of Cu(511) electrode surface from polycrystalline Cu · *Operando* electrochemical scanning tunneling microscopy (OECSTM) · Differential electrochemical mass spectrometry (DEMS) · *Seriatim* OECSTM-DEMS

Introduction

Studies on the heterogeneous electrochemical reduction of CO₂ in aqueous solutions have established that Cu is the only element that delivers a remarkable variety of reduced organic compounds [1–5]. Such a diversity in the product distribution, however, is a disadvantage if only one particular species were sought. Efforts are thus underway for the search of CO₂ reduction (CO₂R) electrocatalysts better than Cu in terms of selectivity [6–9]. However, because of a nagging absence of fundamental principles on the design of selective CO₂R catalysts, interest in Cu remains high. Computationally, the focus has been on reaction mechanisms at well-defined surfaces [10–13], but the studies lack fidelity because they have not accounted for the fact that, under CO₂R conditions, the electrode surface is dynamic and is prone to reconstruction to a different structure [14]. Experimentally, the impetus is on surface modification, compositionally [15, 16] or structurally [17, 18]¹.

The influence of electrode-surface structure on the reduction of CO has been investigated [11–13, 19–21]. The choice of CO as the reactant in lieu of CO₂ is predicated by the fact

✉ Manuel P. Soriaga
msoriaga@caltech.edu

¹ Division of Chemistry and Chemical Engineering, Joint Center for Artificial Photosynthesis, California Institute of Technology, Pasadena, CA 91125, USA

² Department of Chemistry, Texas A&M University, College Station, TX 77843, USA

¹ Other aspects investigated, such as the use of non-aqueous solvent, the employment of reactant concentrators, the influence of electrolyte, the adoption of gas-phase-feed approaches, or the method of product analysis, are deemed not of fundamental significance since those do not alter the free-energy landscape of the electrocatalytic reaction.

that it is the first isolable product and intermediate in the cathodic reduction of CO_2 ; moreover, the pH of the electrolyte solution is independent of CO concentration. None of the studies involved *operando* methodologies that interrogate the Cu surface under catalytic-reaction conditions. In most cases, surface structural information was acquired only prior to the electrolysis; in a few instances, ex situ post-catalysis examinations were also carried out [22].² A seminal work [19, 24] involved the production of ethanol from CO_2 at stepped Cu(100) surfaces, although at a rather large overpotential of 1.13 V. Under such condition, the reduction was not ethanol-product selective because more than ten other products, such as methane and ethylene, were also generated. Nevertheless, the production of ethanol was reported to be optimal for the following stepped surfaces: $\text{Cu}(\text{S})-[n(100)\times(111)]$, when $n=3, 5, \text{ and } 6$, with a Faradaic efficiency of *ca.* 15 % and $\text{Cu}(\text{S})-[n(100)\times(110)]$, when $n=3, 5, 6, \text{ and } 8$, with a Faradaic efficiency of *ca.* 27 %; no information was provided with regard to the surface structures under reaction conditions. A more recent study claimed that reduction of CO on Cu(911), or $\text{Cu}(\text{S})-[5(100)\times(111)]$, selectively produced ethylene at lower potentials; however, the *operando* surface structure was not known [12]. The reduction of CO to $\text{C}_2\text{H}_5\text{OH}$ has also been investigated using so-called oxide-derived (OD) copper [25]. Preparation of the OD Cu involved extensive oxidation of an electropolished polycrystalline Cu foil in a muffle furnace at 500 °C for 1 h in the presence of air, followed by reduction of the oxide back to Cu either by in situ reduction during the reduction of carbon monoxide (COR), or by heat treatment in a tube furnace at 130 °C for 2 h while $\text{H}_2(\text{g})$ was streamed at $100 \text{ cm}^3 \text{ min}^{-1}$. The average roughness factors (RF) that resulted from the former and latter reduction procedures were 135 and 48, respectively. In 0.1 M KOH and at an overvoltage of 485 mV, the rougher OD Cu was reported to generate ethanol selectively at a Faradaic efficiency of 42.9 % but with an activity of only $0.92 \mu\text{A cm}^{-2}$ based on the electrochemically active surface area [25]; the less roughened sample yielded an efficiency of 25.5 % and activity of $0.96 \mu\text{A cm}^{-2}$. Ex situ high-resolution transmission electron microscopy of the post-electrolysis OD Cu was not able to identify the particular structure of the Cu surface. Grain boundaries were, however, discernible and were thought to be responsible for the selective catalysis. As evidence, it was noted that a Cu substrate covered with Cu nanoparticles devoid of grain boundaries showed only paltry catalytic activity [25]. In the context of Cu nanoparticles, a recent study showed that production of hydrocarbons from CO_2 reduction was suppressed, while production of CO and H_2 was enhanced, when the Cu

nanoparticle size was decreased [26]. A discussion had also been made on the influence of nanoparticle size on various modes of catalytic reactions; for example, processes that require terraces and steps are expected to suffer lower activity when the nanoparticle sizes were decreased [27].

The lack of *operando* options precludes a direct correlation, under reaction conditions, between surface structure and catalytic selectivity. This is not a trivial issue because, under $\text{CO}_2\text{R}/\text{COR}$ conditions, Cu undergoes surface reconstruction, as has been recently demonstrated in experiments based on *operando* electrochemical scanning tunneling microscopy (ECSTM). When an electropolished polycrystalline Cu [Cu(pc)] electrode was held at -0.9 V (SHE) in 0.1 M KOH, the surface underwent sequential reconstruction, first to a Cu(111) plane and then to a Cu(100) surface [14]; the reconstructed surface is designated here as $\text{Cu}(\text{pc})-[\text{Cu}(100)]$. The discovery invalidates the hitherto untested notion that the surface structures are the same before, during, and after the electrocatalytic reaction. The experimental flaw, however, may be remedied by the parallel implementation of ECSTM and differential electrochemical mass spectrometry (DEMS), a technique that analyzes products from a surface reaction [6, 28]. The present article describes results from combined *quasi-operando*³ ECSTM-DEMS that made possible the identification of the unique structural constitution of the Cu surface that catalyzes the reduction of CO preferentially to $\text{C}_2\text{H}_5\text{OH}$.

Experimental

Electrochemistry

The electrochemistry experiments for DEMS were conducted with a BioLogic SP-300 potentiostat (BioLogic Science Instruments, Claix, France) equipped for electrochemical impedance spectroscopy (EIS). Potentiostatic EIS measurements were performed at 100 kHz to determine the uncompensated solution resistance (R_u); 85 % of R_u was electronically compensated. The potentiostat used for ECSTM was a built-in component of the Agilent 5500 microscope (Agilent Technologies, Santa Clara, CA). All solutions were prepared using an 18.2 M Ω -cm Nanopure water (ThermoFisher Scientific, Asheville, NC). Potentials were reported with respect to the standard hydrogen electrode (E_{SHE}) rather than the reversible hydrogen electrode (E_{RHE}); the former is directly relatable to thermodynamic free-energy changes and do not

² Cu is a prodigious scavenger of $\text{O}_2(\text{g})$; hence, ex situ characterization of an electrode not stringently protected from the environment will invariably encounter several surface layers of Cu_2O and CuO [23].

³ The appreciable cathodic evolution of H_2 and the reduction of CO at -1.06 V (SHE) precluded the atomic resolution of the ECSTM images. Hence, the ECSTM experiments at slightly less negative potentials (-0.9 V) to ensure minimal catalytic activities, cannot be rigorously classified as true *operando*.

mask pH effects. The interconversion between E_{SHE} and E_{RHE} is given by the relationship: $E_{\text{SHE}} = E_{\text{RHE}} - 0.059 \text{ pH}$.

Electrochemical Scanning Tunneling Microscopy

The electrochemical cell used for STM was custom-crafted from Kel-F (Emco Industrial Plastics, Inc., Cedar Grove, NJ) fitted with a Pt counter electrode and a pre-calibrated Pt quasi-reference electrode [29]. The STM tips were prepared by an electrochemical etch of a 0.25-mm diameter tungsten wire (Sigma-Aldrich, St. Louis, MO) in 0.6 M KOH at 15 VAC. All images were acquired after polarization for an hour in CO-free electrolyte at a constant negative potential (−0.9 V) with a high-resolution scanner in constant-current mode without post-scan processes such as with high-pass filters. The working electrode consisted of either a 99.99 % pure polycrystalline Cu disk (GoodFellow, Coraopolis, PA), 10 mm in diameter and 0.5 mm thick, or a commercially oriented 1.0-mm-thick Cu(100) single crystal, 10 mm in diameter and 99.999 % in purity (Princeton Scientific Corp., Easton, PA). Prior to use, the disk electrode was metallographically polished to a mirror finish with a suspension of polycrystalline diamond (Buehler, Lake Bluff, IL) at a grain size of 0.05 μm. The disk was electropolished in 85 % H₃PO₄ (Sigma-Aldrich) at 2.0 V for 10 s with a Pt counter electrode; it was then ultrasonicated in, and later rinsed with, deaerated Nanopure water. The polished sample, however, was not thermally annealed. The alkaline solution, 0.1 M KOH, used in this study was prepared from analytical-grade KOH reagent (Sigma-Aldrich); it was purged for at least 1 h in oxygen-free, ultrahigh purity argon (Airgas, Radnor, PA).

The root mean square roughness (R_{RMS}) was calculated, with the use of the WSxM software [30], from the surface height data, z_i , obtained from multiple ECSTM images of a given size (e.g., 200 nm × 200 nm or 50 nm × 50 nm). R_{RMS} is an amplitude parameter for roughness, defined in the equation: $R_{\text{RMS}} = \left[\frac{1}{N} \sum_{i=1}^N |z_i - \bar{z}|^2 \right]^{1/2}$; it describes vertical deviations from the mean height \bar{z} . It is important to note that R_{RMS} is a function of the dimensions of the ECSTM image. For a 200 nm × 200 nm image, for example, R_{RMS} was 1.8 nm; for 50 nm × 50 nm, R_{RMS} was 0.2 nm; and for 5 nm × 5 nm, R_{RMS} was 0.02 nm. The latter value is a more realistic depiction of atomic smoothness since it presents the finest (atomic-level) irregularities. The R_{RMS} for the larger (200 nm × 200 nm) segment represents the waviness, or the more widely spaced deviations, of a surface from its nominal shape [31].

Differential Electrochemical Mass Spectrometry

The general principles of DEMS, along with applications to electrochemical surface science, have been amply discussed

elsewhere [32, 33]. The disk electrodes used in the DEMS experiments consisted of (i) a 99.99 % pure polycrystalline Cu disk (Goodfellow, Coraopolis, PA), 10 mm in diameter and 0.15 mm in thickness, and (ii) a commercially oriented 1.0-mm-thick Cu(100) single crystal, 10 mm in diameter, and 99.9999 % in purity (Princeton Scientific Corp., Easton, PA). Prior to use, the electrodes were metallographically polished and then electropolished for 10 s in 85 % phosphoric acid solution (Sigma-Aldrich, St. Louis, MO) at 2.1 V in a two-electrode configuration with a 99.8 %-pure graphite rod (Alfa Aesar, Ward Hill, MA). After a thorough rinse in Nanopure water, a potential of −0.90 V was applied to the Cu electrode in a N₂-saturated 0.1 M KOH solution (Sigma-Aldrich) for 2 h to quantitatively reduce all surface Cu₂O to metallic copper; a 99.99 % pure Pt wire Goodfellow) was used as the counter electrode. Additional purposeful surface structural modifications, such as Cu(pc)-[Cu(100)] reconstruction [14], employed procedures employed in the the ECSTM studies.

The discretely prepared Cu electrode, with a protective layer of electrolyte, was then transferred to the DEMS cell fabricated out of polyether ether ketone, as described previously [6]. A 20-μm-thick polydimethylsiloxane (PDMS) membrane with a 20-nm porosity isolated the electrochemical cell from the mass spectrometry compartment, and a 50-μm glass spacer separated the Cu electrode from the PDMS membrane that resulted in a thin-layer electrochemical cell with a volume of 5.0 μL. A porous glass frit placed between the Cu cathode and Pt anode electrodes precluded the oxidation of the CO-reduction products. The potential of the Cu electrode was held at −1.06 V for 600 s while the reduction products were monitored by an HPR-20 quadrupole mass spectrometer (Hiden Analytical, Warrington, England) with a secondary electron multiplier (SEM) detector with a voltage of 950 V and an emission current of 50 μA. It must be noted that, in DEMS, only species that are hydrophobic and/or volatile can be readily monitored; hence, methane is easily detectable, but products such as acetates cannot be assayed.

The parallel implementation of DEMS and ECSTM involved *separate* experimental setups that shared identical electrochemical pretreatment and catalysis conditions. At least three separate trials were performed with ECSTM, and subsequent runs with DEMS were done twice.

Surface Oxidation-Reduction Cycles

Prior to the combined ECSTM–DEMS experiments, the ordered electrodes were subjected to mild (monolayer-limited) oxidation-reduction cycles (ORC) via multiple voltammetric scans, at 50 mV s^{−1}, between 0.1 and −0.9 V. The intent was to induce controllable surface transformations and determine whatever influences are imparted on the product distribution. At 0.1 V, a single layer of copper(I) oxide, was formed; at −0.9 V, the surface oxide

Operando ECSTM-CV of Cu(100) in 0.1 M KOH

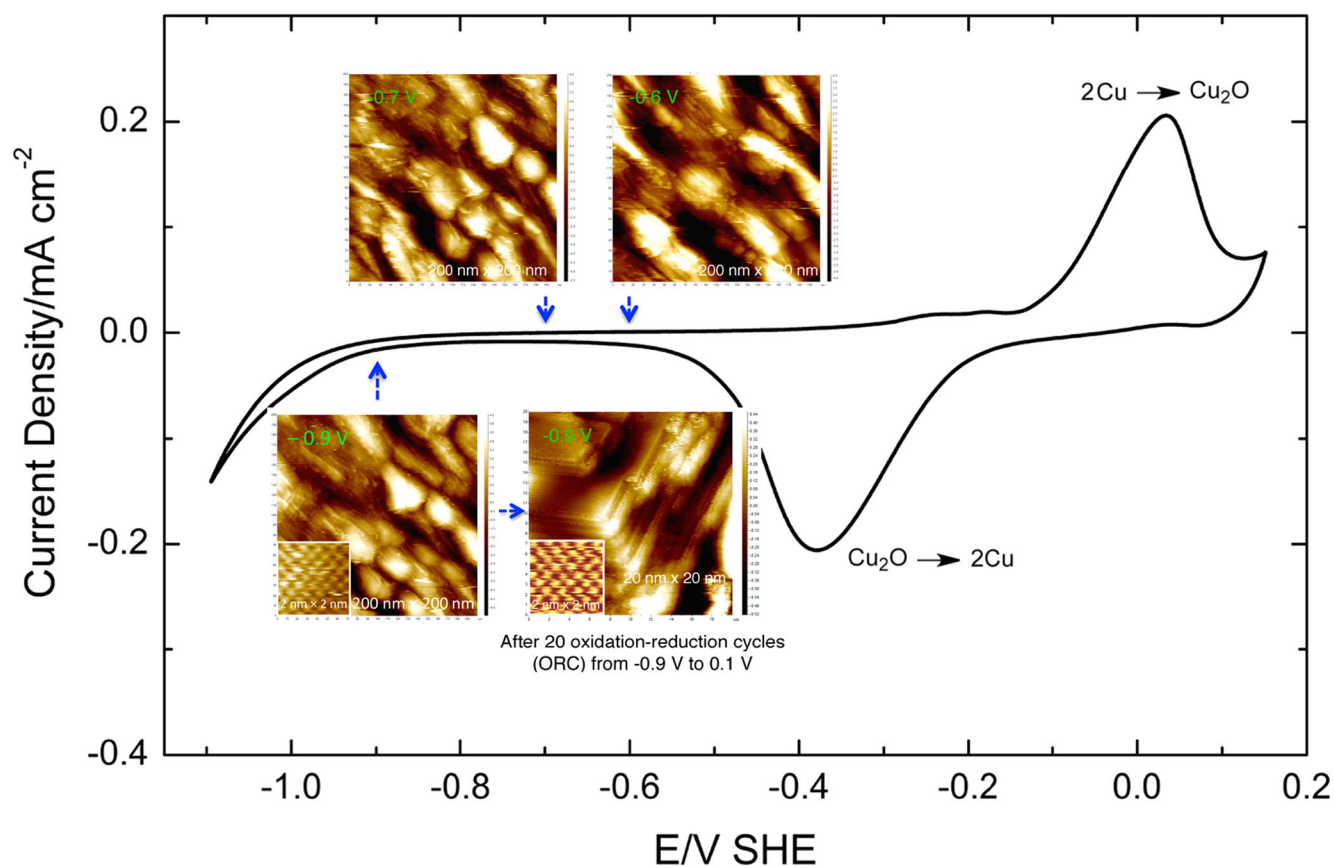


Fig. 1 Simultaneous *operando* electrochemical scanning tunneling microscopy (OECSTM) and cyclic voltammetry (CV) of a well-defined Cu(100) single-crystal surface in 0.1 M KOH solution, before and after multiple oxidation-reduction cycles between 0.1 and -0.9 V. OECSTM

was reduced back to Cu [23]. Excursions to more positive potentials were expected to yield multilayers of copper(II) oxide, which, upon reduction, would lead to extensive surface roughness that then precluded ECSTM experiments [14]. In contrast, the chosen potential window for the present ORC treatment induced critical structural transformations discernible by ECSTM.

Results and Discussion

Figure 1 shows a steady-state cyclic voltammogram (CV) of a well-ordered Cu(100) electrode surface that had been kept at -0.9 V in 0.1 M KOH for 60 min; the current-potential scans were conducted while the electrode was inside the ECSTM cell. As discussed in detail elsewhere [23], the anodic peak at 0.03 V represents the monolayer-limited formation of surface copper(I) oxide, $\text{Cu}_{(s)} \rightarrow \text{Cu}_2\text{O}_{(s)}$, on Cu(100), whereas the cathodic peak at -0.4 V is for the reduction of $\text{Cu}_2\text{O}_{(s)}$ back to metallic copper. Also shown in Fig. 1 are low-resolution (200 nm \times 200 nm), medium-resolution (20 nm \times 20 nm),

images were obtained while the voltammetric plots were being acquired. The geometric area of the single crystal was 1.0 cm², and the potential sweep rate was 50 mV s⁻¹

and high-resolution (2 nm \times 2 nm) ECSTM images⁴ of the oxide-free surface at pre-selected potentials. No distinctive images could be acquired at potentials more positive than -0.4 V because copper(I) oxide starts to emerge and, even at residual surface concentrations, proper engagement of the STM tip is already hindered [23]. More negative potentials were likewise inaccessible by ECSTM because of the deleterious interference by the hydrogen-evolution reaction (HER).

It is important to note that the image of the Cu(100) plane at -0.9 V is not that of a surface roughened by or littered with isolated islands. This is best clarified by progressive low-to-high-resolution images, from 200 \times 200 nm, to 20 nm \times 20 nm, to 10 nm \times 10 nm, and to 2 nm \times 2 nm (Fig. 2). The *operando* ECSTM images indicate that the surface consists essentially of sub-micron-sized Cu(100)

⁴ It cannot be overemphasized that, whereas the ECSTM images displayed in this paper are only for nanometer-scale domains on the bulk crystal, those are representative of the entire surface because numerous images have been evaluated throughout the macroscopic surface. The protocol has always been that results will be adopted only if satisfactory agreement exists among all the sampled images.

Operando EC-STM Images of Cu(100) at -0.9 V in 0.1 M KOH

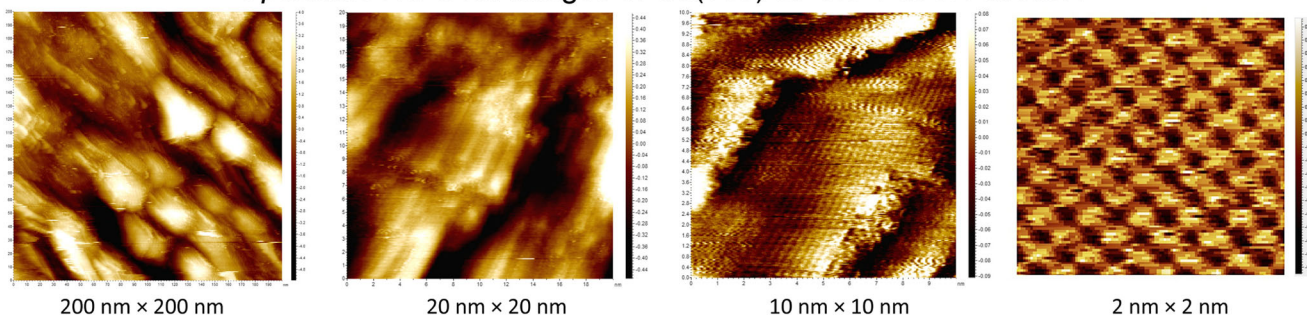


Fig. 2 Operando electrochemical scanning tunneling microscopy (OECSTM) images, progressively increased in resolution, of the

Cu(100) single-crystal electrode held at -0.90 V (SHE) in 0.1 M KOH for 60 min. Experimental conditions were as in Fig. 1

domains each composed of *ca.* 10-nm-wide terraces segregated by monoatomic steps. The terraces are relatively narrow almost certainly because the Cu single crystal had not been previously thermally annealed, but the (100) arrangement of surface atoms on the terraces is easily discerned in the 10-nm-square image. The zoomed-in atom-resolved (2 nm \times 2 nm) ECSTM image, also shown in the inset of Fig. 1 at -0.9 V,

reveals a highly ordered square (1×1) lattice; the interatomic distance was measured to be 0.27 ± 0.01 nm, a value identical to that for a pristine, oxide-free square Cu(100) net [34].

The data in Fig. 1 indicated no drastic changes in the STM images when the applied potential was increased from -0.9 to -0.7 to -0.6 V, or decreased vice versa. That is, within the potential regime where neither oxide nor hydride exists on the

OECSTM-CV of Cu(pc)-[Cu(100)] in 0.1 M KOH

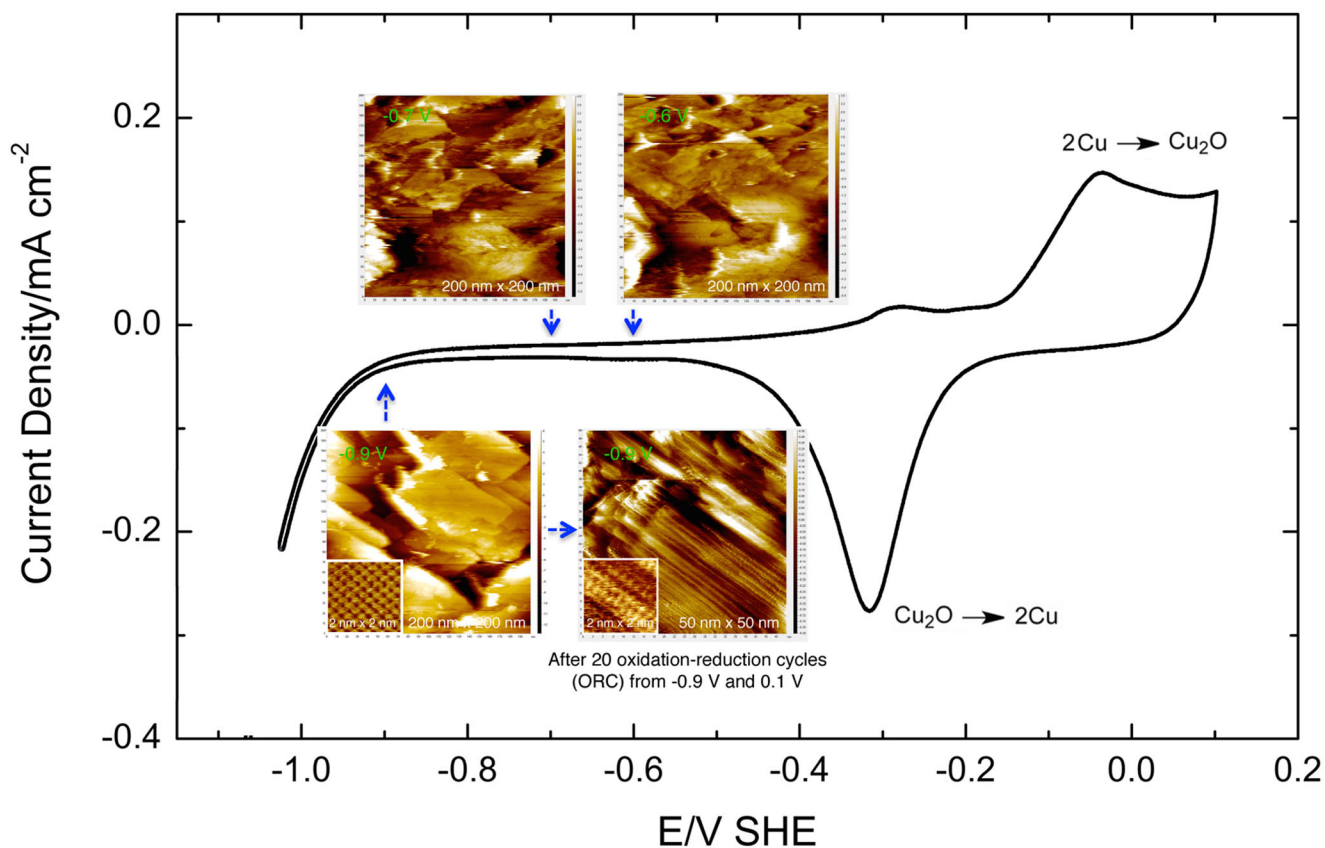


Fig. 3 Simultaneous operando electrochemical scanning tunneling microscopy (OECSTM) and cyclic voltammetry (CV), before and after multiple oxidation-reduction cycles (ORC) in 0.1 M KOH, of a polycrystalline copper electrode, Cu(pc), that had been reconstructed to

a well-defined Cu(100) single-crystal surface, Cu(pc)-[Cu(100)], at -0.9 V in 0.1 M KOH. The OECSTM images were obtained while the voltammetric plots were being acquired. Experimental conditions were as in Fig. 1

surface, an ordered Cu(100) was exceptionally stable. More remarkable perhaps was the resiliency of the Cu(100) single-crystal surface, as manifested by the fact that voltammetric excursions into the $\text{Cu}_2\text{O}_{(s)}$ region failed to disrupt the highly ordered atomic arrangement at the terraces when the potential was switched back to -0.9 V [23]. It is equally important to mention that the voltammetric anodic and cathodic peaks from the first to the twentieth cycles were all identical in morphology and size, a result which signified that the Cu(100) surface was unroughened by the monolayer-restricted ORC. Further corroboration was provided by the root-mean-square roughness, R_{RMS} , of 0.02 nm for the $5\text{ nm} \times 5\text{ nm}$ ECSTM image. The roughness factor, R_{F} , was thus taken as essentially unity, even after multiple ORC.

The corresponding ECSTM-CV for the reconstructed Cu(pc)–[Cu(100)] electrode surface [14] is shown in Fig. 3. The morphology of the CV is not identical to, but faintly differs, from that of the original Cu(100) electrode; it is because, even after only the first oxidation, the structure of the reconstructed surface is no longer that of pure Cu(100). The dissimilarities are more notable for the ECSTM images, such as the sizes of the terraces that are much wider for the reconstructed Cu(pc)–[Cu(100)] surface; however, the pre-ORC atom-resolved ($2\text{ nm} \times 2\text{ nm}$) image at -0.9 V reveals that the wider planes, as with the narrower Cu(100) terraces, are populated only by square (100)-arranged atoms. The most

significant difference is that the post-ORC image for Cu(pc)–[Cu(100)] is no longer the same as for pure Cu(100), a result that supports the explanation above as to why the ECSTM-CVs in Figs. 1 and 3 are non-identical. One similarity is the constancy of the ORC peak areas, regardless of the number of cycles, and the minimal ECSTM R_{RMS} values; hence, the reconstructed Cu(pc)–[Cu(100)] surface was likewise considered as atomically smooth.

Figure 4 showcases the results from the implementation of sequential or *seriatim* ECSTM-DEMS for the generation of ethanol at a post-ORC original Cu(100), Fig. 4a; a pre-ORC reconstructed Cu(pc)–[Cu(100)], Fig. 4b; and a post-ORC Cu(pc)–[Cu(100)], Fig. 4c. At the top of each figure are shown DEMS data in terms of the time dependence of the ion current for $\text{C}_2\text{H}_5\text{OH}$ at a fixed reduction potential, -1.06 V, for the mass-to-charge ratio (m/z) of 31; at the bottom are the associated ECSTM images, which, except for the inset images, are of different resolutions. The arrows signify the potentials at which the DEMS and ECSTM measurements were conducted. It first needs to be noted that: (i) The ECSTM and DEMS measurements were undertaken separately, but in parallel, since it is obvious that both cannot be performed in the same apparatus; to mitigate divergences, the material sources, the surface preparations, and the electrochemical pretreatments prior to the experiments were forged to be identical. (ii) The ECSTM images displayed were

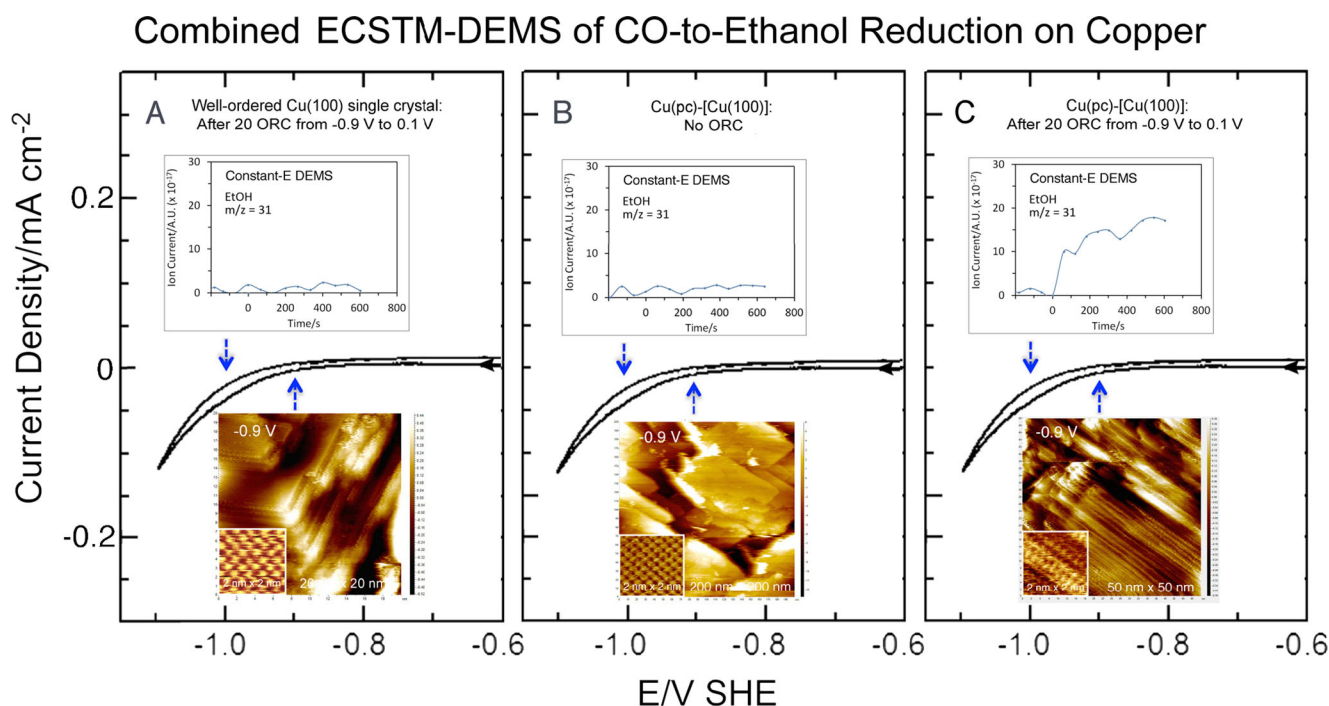


Fig. 4 Combined (sequential) *quasi-operando* electrochemical scanning tunneling microscopy (ECSTM) and differential electrochemical mass spectrometry (DEMS) of a 0.1 M KOH solution saturated with CO at **a** a well-defined Cu(100) single-crystal after multiple oxidation-reduction cycles (ORC), **b** a reconstructed Cu(pc)–[Cu(100)] without prior ORC, and **c** a reconstructed Cu(pc)–[Cu(100)] after multiple ORC. The

potentials for the DEMS and ECSTM measurements are indicated by the *arrows*. The DEMS signals were only for $\text{C}_2\text{H}_5\text{OH}$ as the product. The ECSTM images were identical before and after potential excursions to -1.06 V, in the absence of CO in solution; no images could be obtained at that potential because of deleterious effects by the onset of the hydrogen evolution reaction and CO reduction

acquired at -0.9 V, and not at -1.06 V, since, at the latter potential, only inferior images were possible due to initiation of the hydrogen evolution reaction. However, when the electrodes were brought to a potential of -1.06 V, but without the ECSTM measurements, and then returned to -0.9 V, no changes were observed in the original images. (iii) The reduction is in 0.1 M KOH at a rather low potential, 645 mV less negative than that required for the formation of multiple highly reduced products such as CH_4 or C_2H_4 [1, 5]. (iv) Both ethanol and methanol yield ion currents at $m/z=31$, but ethanol gives an additional MS signal at $m/z=45$. Methanol also has a substantial secondary peak at 32, although in the DEMS apparatus, it is obscured by the large signal from residual oxygen. The absence of methanol was inferred from the observation that the ratio of the ethanol signals at m/z of 31 and 45 was the same as that for a CH_3OH -free $\text{C}_2\text{H}_5\text{OH}$ standard. The signal at $m/z=31$ was chosen for DEMS quantification because it has the higher signal-to-noise ratio.

The well-ordered $\text{Cu}(100)$ surface did not generate ethanol (or other products like methane and ethylene) under the present conditions as indicated by the fact that the DEMS results (Fig. 4a) before and after ORC were identical. As already noted in Fig. 1, multiple oxidation-reduction treatments were unable to disrupt the pristine atomic arrangement of the $\text{Cu}(100)$ surface; hence, it came as no surprise that the post-ORC $\text{Cu}(100)$ surface did not exhibit catalytic activity. The inertness of the ordered $\text{Cu}(100)$ surface is further confirmed by the data in Fig. 4b for the pre-ORC $\text{Cu}(\text{pc})$ - $[\text{Cu}(100)]$: The reconstructed $\text{Cu}(\text{pc})$ - $[\text{Cu}(100)]$ that was not subjected to ORC remained (100)-ordered and, likewise failed to catalyze the CO -to- $\text{C}_2\text{H}_5\text{OH}$ reduction. On the other hand, the application of multiple ORC on $\text{Cu}(\text{pc})$ - $[\text{Cu}(100)]$ induced a further slight reconstruction⁵ to a different structure grounded largely on the original $\text{Cu}(100)$ motif; as the highlight in the DEMS spectrum in Fig. 4c, such an ordered stepped surface generated ethanol.

The quantity of ethanol produced was determined by external calibration in which the MS ion current was plotted as a function of the solution concentration of ethanol standards. The average over the 600-s constant-potential electrolysis was found to be 4.0 mM, for which the equivalent activity was $24 \mu\text{A cm}^{-2}$ based on the geometric area and R_F of one. The current efficiency, 31 %, was computed from the number of coulombs needed to generate the measured amount of ethanol divided by the total electrolytic charge passed.

⁵ It is not understood at this time, but it is beyond the scope of the present paper, why an ordered $\text{Cu}(100)$ layer situated at the top of a $\text{Cu}(\text{pc})$ substrate is more pliable than a $\text{Cu}(100)$ sheet above a $\text{Cu}(100)$ base. It is likely related to the adhesion of various surfaces in contact with one another. For example, the adhesion coefficient of $\text{Cu}(100)$ - $\text{Cu}(100)$ planes has been reported to be five times larger than that for $\text{Cu}(111)$ - $\text{Cu}(100)$ surfaces [35].

The selective or preferential production of ethanol over methane and ethylene from the electrochemical reduction of carbon monoxide is portrayed by the *seriatim* ECSTM-

Ethanol-product Selectivity of Post-ORC $\text{Cu}(\text{pc})$ - $[\text{Cu}(100)]$ at -1.0 V in 0.1 M KOH

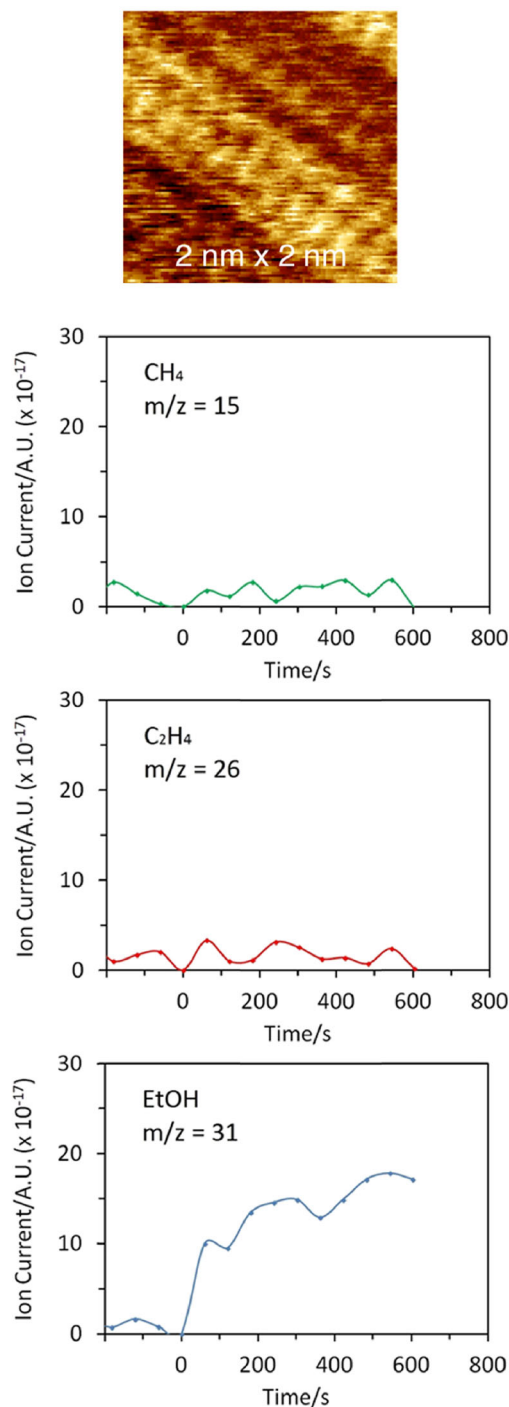


Fig. 5 Differential electrochemical mass spectrometry (DEMS) for a post-oxidation-reduction cycle (ORC) reconstructed $\text{Cu}(\text{pc})$ - $[\text{Cu}(100)]$ at -1.06 V in a 0.1 M KOH solution saturated with CO . The DEMS signals were for CH_4 , C_2H_4 , and $\text{C}_2\text{H}_5\text{OH}$ as products

DEMS data in Fig. 5: At an overpotential of 485 mV in 0.1 M KOH electrolyte, the catalysis by the post-ORC Cu(pc)–[Cu(100)] surface shows only C₂H₅OH as a product. If the reduction overpotential was made more negative, other hydrocarbons would be generated; the more negative the applied potential, the higher the yield of all the products, but the worse the selectivity [1].

The present investigation has offered an atomic-level view of the particular Cu surface that may persist during the selective reduction of CO to ethanol at low overpotentials. This accomplishment has been facilitated most likely by the facts that well-ordered surfaces were employed initially, and that the perturbations to induce catalytic activity were kept to a minimum so as not to stifle ECSTM experiments. Fig. 6 shows a zoomed-in ECSTM image of the ethanol-product-selective Cu surface; a 5 nm × 5 nm square image is displayed since a 2 nm × 2 nm area highlights only the terraces but not the steps (*cf.*, Fig. 2). A careful examination of the image reveals a terrace occupied by three rows of Cu(100) atoms and a monoatomic step of Cu(111) atoms. The structure is that of a stepped surface, Cu(S)–[3(100) × (111)] or, in shorter notation, Cu(511). The model crystal lattice for such stepped structure is also shown in Fig. 6. The fact that Cu(100) and Cu(111) single-crystal electrodes do not yield ethanol in alkaline solution at low overpotentials, is indicative of the critical role of surface steps and terraces in C–C bond formation. The use of well-defined stepped surfaces of Cu provides a dynamic arena for further

implementation of *operando* ECSTM-DEMS to gain mechanistic insights into the surface-site sensitivity of the selective conversion of CO into highly reduced organic compounds.

Summary and Conclusions

The catalysis by copper of the electrochemical reduction of CO₂ or CO to a variety of products is an unwelcome attribute when only one reduced organic compound is sought. The present study provides an example in which, through the atomic-level structural modification of the Cu electrode surface, the product distribution is regulated to yield only one major compound. The reaction investigated was the preferential reduction of CO to C₂H₅OH on Cu at a low overpotential in alkaline solution. Experimental measurements combined *quasi-operando* electrochemical scanning tunneling microscopy and differential electrochemical mass spectrometry. An atomically smooth and well-ordered Cu(100) surface, prepared from either a single crystal or by Cu(pc)-to-Cu(100) reconstruction, did not produce ethanol. When the surfaces were subjected to monolayer-limited oxidation-reduction cycles, only the Cu(pc)–[Cu(100)] surface underwent an additional, albeit minor, structural reconstruction that spawned the selective generation of ethanol at a potential 645 mV lower than that which generates multiple products. A Faradaic efficiency of 31 % and an activity of 24 μA cm⁻² were measured;

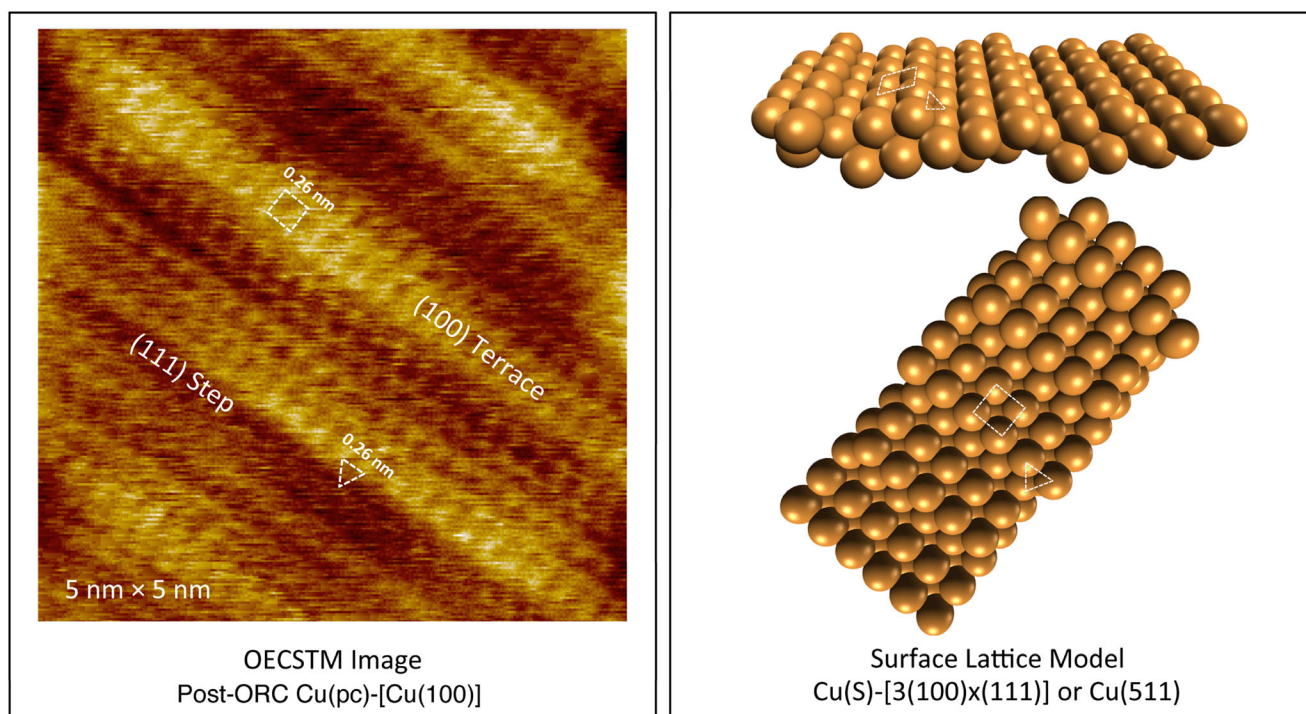


Fig. 6 *Left:* High-resolution *quasi-operando* electrochemical scanning tunneling microscopy (OECSTM) image of the post-oxidation-reduction cycle (ORC) reconstructed Cu(pc)–[Cu(100)] surface that

depicts a three-row terrace of Cu(100) and a one-atom step of Cu(111). *Right:* The ideal surface lattice model of the stepped Cu(S)–[3(100) × (111)] or Cu(511) surface

neither methane nor ethylene was generated. ECSTM indicated that the transformation was to an ordered stepped surface, Cu(S)–[3(100)×(111)], or Cu(511). The inference is that the non-selective, multiple-product electrocatalytic reduction of CO can be regulated to yield only one organic compound through the nanometer-scale structural control of the Cu surface.

Acknowledgments This material is based upon work performed by the Joint Center for Artificial Photosynthesis, a DOE Energy Innovation Hub, supported through the Office of Science of the U.S. Department of Energy under Award No. DE-SC0004993.

References

1. Y. Hori, Electrochemical CO₂ reduction on metal electrodes, in *Modern Aspects of Electrochemistry*, ed. by C.G. Vayenas, R.E. White, M.E. Gamboa-Aldeco (Springer, New York, 2008), p. 89
2. M. Gattrell, N. Gupta, A. Co, A review of the aqueous electrochemical reduction of CO₂ to hydrocarbons at copper. *J Electroanal Chem* **594**, 1 (2006)
3. D.T. Whipple, P.J.A. Kenis, Prospects of CO₂ utilization via direct heterogeneous electrochemical reduction. *J Phys Chem Lett* **1**, 3451 (2010)
4. K.J.P. Schouten, Y. Kwon, C.J.M. van der Ham, Z. Qin, M.T.M. Koper, A new mechanism for the selectivity to C₁ and C₂ species in the electrochemical reduction of carbon dioxide on copper electrodes. *Chem Sci* **2**, 1902 (2011)
5. K.P. Kuhl, E.R. Cave, D.N. Abram, T.F. Jaramillo, New insights into the electrochemical reduction of carbon dioxide on metallic copper surfaces. *Energy Environ Sci* **5**, 7050 (2012)
6. A. Javier, J.H. Baricuatro, Y.-G. Kim, M.P. Soriaga, Overlayer Au-on-W near-surface alloy for the selective electrochemical reduction of CO₂ to methanol: empirical (DEMS) corroboration of a computational (DFT) prediction. *Electrocatalysis* **6**, 493 (2015)
7. S. Back, H. Kim, Y. Jung, Selective heterogeneous CO₂ electroreduction to methanol. *ACS Catal* **5**, 965 (2015)
8. M. Karamad, V. Tripkovic, J. Rossmeisl, Intermetallic alloys as CO electroreduction catalysts—role of isolated active sites. *ACS Catal* **4**, 2268 (2014)
9. K. Chan, C. Tsai, H.A. Hansen, J.K. Nørskov, Molybdenum sulfides and selenides as possible electrocatalysts for CO₂ reduction. *ChemCatChem* **6**, 1899 (2014)
10. J.H. Montoya, C. Shi, K. Chan, J.K. Nørskov, Theoretical insights into a CO dimerization mechanism in CO₂ electroreduction. *J Phys Chem Lett* **6**, 2032 (2015)
11. T. Cheng, H. Xiao, W.A. Goddard, Free-energy barriers and reaction mechanisms for the electrochemical reduction of CO on the Cu(100) surface, including multiple layers of explicit solvent at pH 0. *J Phys Chem Lett* **6**, 4767 (2015)
12. K.J.P. Schouten, Z. Qin, E.P. Gallent, M.T.M. Koper, Two pathways for the formation of ethylene in CO reduction on single-crystal copper electrodes. *J Am Chem Soc* **134**, 9864 (2012)
13. F. Calle-Vallejo, M.T.M. Koper, Theoretical considerations on the electroreduction of CO to C₂ species on Cu(100) electrodes. *Angew Chem Int Ed* **52**, 7282 (2013)
14. Y.-G. Kim, J.H. Baricuatro, A. Javier, J.M. Gregoire, M.P. Soriaga, The evolution of the polycrystalline copper surface, first to Cu(111) and then to Cu(100), at a fixed CO₂RR potential: A study by operando EC-STM. *Langmuir* **30**, 15053 (2014)
15. E. Andrews, M. Ren, F. Wang, Z. Zhang, P. Sprunger, R. Kurtz, J. Flake, Electrochemical reduction of CO₂ at Cu nanocluster/(100) ZnO electrodes. *J Electrochem Soc* **160**, H841 (2013)
16. D. Kim, J. Resasco, Y. Yu, A.M. Asiri, P. Yang, Synergistic geometric and electronic effects for electrochemical reduction of carbon dioxide using gold-copper bimetallic nanoparticles. *Nat Commun* **5**, 4948 (2014)
17. S. Zhu, M. Shao, Surface structure and composition effects on electrochemical reduction of carbon dioxide. *J Solid State Electrochem* **20**, 861 (2015)
18. W. Tang, A.A. Peterson, A.S. Varela, Z.P. Jovanov, L. Bech, W.J. Durand, S. Dahl, J.K. Nørskov, I. Chorkendorff, The importance of surface morphology in controlling the selectivity of polycrystalline copper for CO₂ electroreduction. *Phys Chem Chem Phys* **14**, 76 (2012)
19. Y. Hori, I. Takahashi, O. Koga, N. Hoshi, Selective formation of C₂ compounds from electrochemical reduction of CO₂ at a series of copper single crystal electrodes. *J Phys Chem B* **106**, 15 (2002)
20. Y. Hori, R. Takahashi, Y. Yoshinami, A. Murata, Electrochemical reduction of CO at a copper electrode. *J Phys Chem B* **101**, 7075 (1997)
21. Y. Hori, A. Murata, R. Takahashi, S. Suzuki, Electroreduction of carbon monoxide to methane and ethylene at a copper electrode in aqueous solutions at ambient temperature and pressure. *J Am Chem Soc* **109**, 5022 (1987)
22. A. Verdaguier-Casadevall, C.W. Li, T.P. Johansson, S.B. Scott, J.T. McKeown, M. Kumar, I.E.L. Stephens, M.W. Kanan, I. Chorkendorff, Probing the active surface sites for CO reduction on oxide-derived copper electrocatalysts. *J Am Chem Soc* **137**, 9808 (2015)
23. Y.-G. Kim, M.P. Soriaga, Cathodic regeneration of a clean and ordered Cu(100)-(1 × 1) surface from an air-oxidized and disordered electrode: an operando STM study. *J Electroanal Chem* **734**, 7 (2014)
24. Y. Hori, I. Takahashi, O. Koga, N. Hoshi, Electrochemical reduction of carbon dioxide at various series of copper single crystal electrodes. *J Mol Catal A Chem* **199**, 39 (2003)
25. C.W. Li, J. Ciston, M.W. Kanan, Electroreduction of carbon monoxide to liquid fuel on oxide-derived nanocrystalline copper. *Nature* **508**, 504 (2014)
26. R. Reske, H. Mistry, F. Beharfarid, B. Roldan Cuenya, P. Strasser, Particle size effects in the catalytic electroreduction of CO₂ on Cu nanoparticles. *J Am Chem Soc* **136**, 6978 (2014)
27. R.A. van Santen, Complementary structure sensitive and insensitive catalytic relationships. *Acc Chem Res* **42**, 57 (2009)
28. A. Javier, B. Chmielowiec, J. Sanabria-Chinchilla, Y.-G. Kim, J.H. Baricuatro, M.P. Soriaga, A DEMS study of the reduction of CO₂, CO, and HCHO pre-adsorbed on Cu electrodes: empirical inferences on the CO₂RR mechanism. *Electrocatalysis* **6**, 127 (2015)
29. K. Itaya, In situ scanning tunneling microscopy in electrolyte solutions. *Prog Surf Sci* **58**, 121 (1998)
30. I. Horcas, R. Fernández, J.M. Gomez-Rodriguez, J. Colchero, J. Gómez-Herrero, A.M. Baro, WSXM: a software for scanning probe microscopy and a tool for nanotechnology. *Rev Sci Instrum* **78**, 013705 (2007)
31. T.V. Vorburger, Methods for Characterizing Surface Topography, in: *Tutorials in Optics*, ed. by D.T. Moore (Optical Society of America, Washington, DC, 1992), p. 137
32. H. Baltruschat, Differential Electrochemical Mass Spectrometry as a Tool for Interfacial Studies, in: *Interfacial Electrochemistry*, ed. by A. Wieckowski (Marcel Dekker, New York, 1999), p. 577
33. H. Baltruschat, Differential electrochemical mass spectrometry. *J Am Soc Mass Spectrom* **15**, 1693 (2004)
34. R.W.G. Wyckoff, *Crystal Structures*, vol. 1, 2nd edn. (Wiley, New York, 1963)
35. D.H. Buckley, *Surface Effects in Adhesion, Friction, Wear, and Lubrication* (Elsevier, New York, 1981), p. 270